Scalable high-affinity stabilization of magnetic iron oxide nanostructures by a biocompatible antifouling homopolymer

Giovanni Luongo[1], Paola Campagnolo[1,2], Jose E. Perez[3], Jürgen Kosel[3], Theoni K. Georgiou[1], Anna Regoutz[1], David J. Payne[1], Molly M. Stevens[1,4], Mary P. Ryan[1], Alexandra E. Porter[1], and Iain E. Dunlop[1]*

[1] Department of Materials, Imperial College London, London SW7 2AZ, United Kingdom.

[2] School of Biosciences and Medicine, Faculty of Health and Medical Sciences, University of Surrey, Guildford, GU2 7XH.

[2] King Abdullah University of Science and Technology, Thuwal 23955, Kingdom of Saudi Arabia.

[4] Department of Bioengineering and Institute for Biomedical Engineering, Imperial College London, London SW7 2AZ, United Kingdom.

* Corresponding Author i.dunlop@imperial.ac.uk

KEYWORDS: magnetic nanoparticles, biocompatible nanoparticles, surface functionalization, iron oxide, magnetite, maghemite, poly(MPC), surface-adsorbed polymers.

Abstract: Iron oxide nanostructures have been widely developed for biomedical applications, due to their magnetic properties and biocompatibility. In clinical application, the stabilization of these nanostructures against aggregation and non-specific interactions is typically achieved using weakly anchored polysaccharides, with better-defined and more strongly anchored synthetic polymers not commercially adopted due to complexity of synthesis and use. Here, we show for the first time stabilization and biocompatibilization of iron oxide nanoparticles by a synthetic homopolymer with strong surface anchoring and a history of clinical use in other applications, poly(2-methacryloyloxyethy phosphorylcholine) (poly(MPC)). For the commercially important case of spherical particles, binding of poly(MPC) to iron oxide surfaces and highly effective individualization of magnetite nanoparticles (20 nm) are demonstrated. Next-generation high-aspect ratio nanowires (both magnetite/maghemite and core-shell iron/iron oxide) are furthermore stabilized by poly(MPC)-coating, with nanowire cytotoxicity at large concentrations significantly reduced. The synthesis approach is exploited to incorporate functionality into the poly(MPC) chain is demonstrated by random copolymerization with an alkyne-containing monomer for click-chemistry. Taking these results together, poly(MPC) homopolymers and random copolymers offer a significant improvement over current iron oxide nanoformulations, combining straightforward synthesis, strong surface-anchoring and well-defined molecular weight.

Introduction

Nanostructures of the magnetic iron oxides magnetite (Fe_3O_4) and maghemite (γ-Fe_2O_3) are of great interest for biomedical applications due to their biocompatibility and magnetic properties, in particular superparamagnetism[1]. Consequently, they have been explored for bioseparation[2,3], magnetically-enhanced drug delivery[4,5], hyperthermic tumor ablation[6,7] and as contrast agents for magnetic resonance imaging (MRI)[8-10]. Beyond the state-of-the art, high-aspect ratio magnetic nanostructures such as nanowires have been found to offer superior performance to spherical nanoparticles for biomedical applications including cell guidance[11], microrheology [12], magnetic cell separation[13] and detection, MRI[14], and mechanically-driven killing of targeted cells[15,16].

For all these applications, the nanoparticles must be coated with a polymeric or small molecule dispersant to stabilize them in solution and reduce non-specific interactions with cells and proteins (*anti-fouling*). Broadly speaking, three coating strategies have been developed[17] Firstly, the use of polymers that combine stabilizing and antifouling properties with weak physisorption to the iron oxide surface (Fig 1A left). This strategy, often implemented with polysaccharides such as dextran, suffers from reversible binding that facilitates bridging between nanoparticle and thus the formation of multiparticle clusters with poor size-control. However its simplicity has made it the approach of choice for the few iron oxide nanoreagents that have reached the market as MRI contrast agents (e.g. ferucarbotran as Resovist®, Cliavist™ and ferumoxide as Feridex®/Endorem®) and as anemia treatments (e.g. Dexferum®)[18]. A more sophisticated approach is to use antifouling polymers such as poly(ethylene glycol) as stabilizing moieties, functionalized at one end with anchoring groups that strongly bind the iron oxide surface, such as dopamine[19,20], silanes[21] and phosphates[22]. This eliminates bridging, but since each polymer molecule is anchored at one point only, the overall affinity with which each molecule is bound

may not be improved with respect to the dextran-type systems, despite the use of higher-affinity surface-anchoring groups. Furthermore, the heterobifunctional molecules required for this method are intrinsically harder to prepare in pure form than homopolymers or random copolymers, especially if there is a need to incorporate for example bioactive molecules at the non-surface-anchored polymer end. A third approach is to adopt a multistep process where the nanoparticles are first functionalized with small-molecules bearing strongly-anchoring functional groups, forming a stable self-assembled monolayer (SAM) onto which end-functionalized polymer molecules can be linked or grown[21] (Fig1A right). This can deliver excellent stability due to the inherent stability of the SAM, but at the cost of a multistep process. Neither multistep processes nor the generation of pure, precisely characterized heterobifunctional polymers are challenging in an academic lab context, however the commercial dominance of simple polysaccharide-based products[17] suggests that such sophisticated syntheses act as barriers to scale-up and clinical translation.

An ideal stabilization platform would thus combine strong anchoring to the substrate with ease of manufacture, suggesting a simple homopolymer containing a strongly anchoring group such as a phosphate. Within this category, we suggest that an outstanding candidate is poly(2-methacryloyloxyethyl phosphorylcholine) (polyMPC) a methacrylate polymer with a phosphorylcholine side-group that resembles the head groups of common biological lipids[23]. This makes polyMPC inherently anti-fouling against protein adsorption[24], with established biocompatibility, including antithrombotic properties[25-28] and an absence of adverse effects in human trials when used as a friction-reducing coating on hip joints[29,30]. Its ability to overcome colloidal forces that drive aggregation has been demonstrated in multistep syntheses where

brush-like poly(MPC) structures have been grown from initiator-functionalized nanoparticles by surface-initiated radical polymerization[21], or created using graft copolymers[31].

In this paper we test the premise that iron oxide nanostructures can, instead, be stabilized by simple adsorption of a polyMPC homopolymer. This is a novel approach that replicates the simplicity of polysaccharide-adsorption with a synthetic polymer, eliminating multistep processes, heterobifunctional linkers and complex polymer architectures, and with a large number of potentially surface-binding groups per chain. In contrast to polysaccharide-adsorption, it delivers a much stronger phosphate-based anchoring to the surface. As will be shown below, poly(MPC) adsorption turns out to be highly effective at generating individualized (20 nm) nanoparticles, whereas the commercial polysaccharide reagents can typically only generate mini-aggregates with multiple particles per polysaccharide molecule[17].

Beyond spherical particles, we investigated poly(MPC) as a stabilizer for next-generation iron oxide nanowires. Despite the clear advantages offered by a low-toxicity magnetite or maghemite nanowire system stabilized with a biocompatible antifouling polymer none is to our knowledge described in the literature. To fill this gap, we synthesized two nanowire systems: a novel super-paramagnetic magnetite (Fe_3O_4) with maghemite (γ-Fe_2O_3) mixture, and a contrasting ferromagnetic nanowire system with an iron core and iron oxide shell[32]. The inherent magnetic moment of such ferromagnetic nanowires makes them extremely susceptible to aggregation, meaning that they have not usually been favored for biomedical applications, however a successful stabilization technology would make their application *in vivo* achievable. Taking this ferromagnetic system as a test case, we investigated the effect of poly(MPC) on cytotoxicity.

Exploiting the advantages of using a synthetic polymer rather than a polysaccharide, we demonstrate the simple incorporation of additional functionalization groups via random co-

polymerization. A prime target application is binding biomolecules to the stabilized particle for cell-targeting, hence a flexible functional group is needed that can be used to attach any desired protein or peptide or antibody. To this end we incorporate alkyne groups that enable biofunctionalization via the alkyne-azide click reaction, which can be carried out with high selectivity under benign aqueous conditions[33-36]. In principle, random incorporation of alkyne groups into a methacrylate polymer such as poly(MPC) simply requires an alkyne-bearing methacrylate monomer such as propargyl methacrylate (PMA). Previous studies show that PMA can interfere with control in some atom transfer radical polymerization (ATRP) systems[37] and a previous attempts to copolymerize PMA with MPC hence trialled silane-protection without success[38]. Here, we show that unprotected PMA, co-polymerized with MPC can generate a clickable random co-polymer, thus delivering stable functionalized iron oxide nanoparticles.

Experimental Section

Materials and Methods

Synthesis of poly(MPC) homopolymer

The synthesis of poly(MPC) by ATRP in protic solvents is well-established, using the cooper-bpy ATRP catalyst system. In general water enables more rapid polymerization and short-chain alkyl alcohols superior control and narrower dispersity [39,40].

Here, poly(MPC) was synthesized in ethanol[41], selected as a more versatile solvent for comonomer incorporation than water. Details of materials are given in Supporting Information (SI). The initiator poly(ethylene glycol) methyl ether 2-bromisobutyrate (initiator Mn 600 kDa, so that the Mn of the PEG section is 350 Da; PEGBr, 1 equiv., 81.0 mg) was dissolved in anhydrous ethanol (10.0 ml) at room temperature with oxygen-free conditions generated by bubbling of nitrogen. Copper (I) Bromide (1 equiv., 19.4 mg) and 2,2'-bipyridine (bpy, 2 equiv.,

42.2 mg) were added and allowed to dissolve, before this solution was added still under nitrogen to 2-methacryloyloxyethyl phosphorylcholine (MPC, 50 equiv., 1.99 g). Upon addition to MPC, a color change was observed from a very dark shade to a mid-green. After 24 hours (due to the slower expected kinetics in ethanol as compared with the standard water synthesis[40]), the polymerization was terminated by exposure to ambient oxygen. The polymer was collected by precipitation in tetrahydrofuran (THF) and centrifugation (10000g, 20 mins), and purified by water dialysis (regenerated cellulose membranes with a 3.5 – 5 kDa cutoff, sample to water ratio 1:400, incubated for 24h with 3 changes of water). Finally, the sample was collected by freeze-drying.

Synthesis of poly(MPC) was confirmed by ^{1}H-NMR in MeOD: δ = 0.91-1.17 (-CH_2-, 2H) 1.85-1.90 (-CH_3, 3H), 3.27-3.37 (-N(CH_3), 9 H), 3.70-3.80 (-CH_2N, 2H), 4.03-4.13 (POCH_2-, 2H) and 4.17-4.40 (OCH_2-CH_2OP, 4H). Further confirmation is provided by the absence of the chemical shifts typical of MPC monomer[9] δ = 5.60 (-CH-, 1H) and 6.10 (CH=, 1H). Molecular mass and dispersity were estimated by aqueous gel permeation chromatography (GPC) calibrated with poly(ethylene glycol) standards, giving an average molecular mass Mn = 8.50 kDa (dispersity Đ = 1.18). Detailed methods and GPC elution curves are given in SI.

Synthesis of poly(MPC-co-PMA) random copolymer

As outlined above, propagryl methacrylate (PMA) was incorporated directly into a random co-polymerization with MPC, without the use of protecting groups. The reaction was carried out as for MPC homopolymer synthesis, except that the initiator/catalyst solution was added to a mixture of MPC (50 equiv. 1.99 g) and PMA (25 equiv. 0.43 g), rather than to MPC (50 equiv.) alone.

The MPC-PMA random copolymer was characterized by ^{1}H-NMR, FTIR and GPC. The ^{1}H-NMR spectrum was identical to that for poly(MPC), confirming a successful polymerization and indicating that PMA had incorporated into the chain at a much lower ratio to MPC than the 1:2 ratio of the reactants. However clear confirmation of PMA incorporation into the poly(MPC) chain is provided by a fluorescence-based assay after click-functionalization.

*Fluorescent labelling of poly(MPC-*co*-PMA) and quantification of functionality*

To demonstrate the creation of functionalized magnetic nanostructures using poly(MPC-*co*-PMA) and to quantify the number of addressable alkyne groups per polymer chain or nanostructures, poly(MPC-*co*-PMA) was reacted with an azide-modified fluorescent dye. Specifically, poly(MPC-co-PMA) was reacted with Azide-Fluor 545 (generic name 5-Carboxytetramethylrhodamine-azide, Sigma Aldrich) in the presence of copper (II) sulphate and sodium ascorbate (ultrapure water, 20 °C, oxygen-free environment generated by nitrogen bubbling, 7 day reaction time). The polymer reaction product was purified by precipitation in THF, dialysis and freeze-drying as for the initial purification following polymer synthesis. A control experiment was performed using poly(MPC) rather than poly(MPC-*co*-PMA) to demonstrate the specificity of the conjugation reaction, and that the azide does not bind to the polymer via other non-covalent interactions.

The number of fluorescent moieties clicked to the poly(MPC-*co*-PMA) was determined using UV-visible spectroscopy at 545 nm (Perkin Elmer Lambda 25 spectrometer). A concentration ladder of Azide-Fluor 545 solutions was used for calibration curve. UV-visible spectra for the labelled polymer, poly(MPC) control and selected calibration solutions are shown in Fig S.2.

Iron oxide nanostructures

Magnetite (iron (II, III)) nanoparticles in aqueous solution were used as received (Sigma-Aldrich). In stability experiments, these were washed to remove stabilizing ligands incorporated by the manufacturer (described as short PEG ligands), as described below.

Magnetite-maghemite nanowires were synthesized by electrodeposition into a commercial polycarbonate template pre-structured with nanochannels, onto which had been sputtered a copper electrode. Electrodeposition was carried out at 90 °C from a mixed solution of ammonium iron(II) sulfate ($(NH_4)_2Fe(SO_4)_2$) and potassium acetate (CH_3COOK). The nanowires were released by first washing with 65% nitric acid to remove the copper electrode, and then repeated rinsing with dichloromethane (DCM) to remove the polycarbonate. The latter step required careful optimization with X-ray photoelectron spectroscopy used to validate the number of washes needed to effectively remove the polycarbonate coating (~ 10 washes). The nanowires were extensively characterized (Supporting Information).

Core-shell iron/iron oxide nanowires were synthesized as previously described[42-44], with some modifications. Briefly, metallic iron was electrodeposited via pulsated current into a porous alumina template, porous alumina template using a solution consisting of 139 g/L $FeSO_4 \cdot 7H_2O$, 24.7 g/L H_3BO_3, 74.5 g/L Na_2SO_4 and 1 g/L $C_6H_8O_6$. A 1M NaOH solution was then used to release the nanowires from the templates[45], with a thin native oxide surface layer surrounding the metallic core[46]. The resulting nanowire population had a length 4.2 ± 0.9 μm, diameter 35.2 ± 1.5 μm, magnetic moment 222 e.m.u./g). This method is versatile and the oxide layer thickness can be controlled through annealing[32].

Poly(MPC) binding and nanoparticle stability

Spherical nanoparticles (20 nm) were used as received and for control samples were washed in water to remove stabilizing ligands from the manufacturer. For poly(MPC)-stabilized samples,

poly(MPC) was added before the washing step to displace the as-supplied ligand molecules. Specifically, as-received stock solution (10μl) was added to either a 5 mg/ml solution of poly(MPC) in water or to water alone, and stirred for 24 h. The nanoparticles were extracted magnetically (Magna-Sep™ Magnetic Particle Separator, 60 mT / cm, ThermoFisher, 3 h incubation). The rinsing procedure was then repeated twice more with water alone, with 10 minutes ultrasonication between each step to break up any temporary aggregates. Samples were then deposited onto a holey carbon TEM grid for analysis (5 µl, left to deposit for 1 – 5 minutes, then blotted with filter paper to leave a thin film that was allowed to air-dry) or prepared for cryo-TEM as described in SI.

Transmission electron microscopy (TEM)

Detailed protocols for all TEM and sample preparation techniques are given in the SI. In brief, the stability of poly(MPC) functionalized and non-functionalized magnetite nanoparticles was investigated using bright-field TEM. Images were taken across a pre-determined area of the surface to avoid operator bias, and each nanoparticle was categorized as either an individual or a member of an aggregate of size *n*. Nanoparticles were considered to belong to the same aggregate if separated by < 20 nm. This approach of measuring aggregation using TEM on dried samples has been previously validated by our group in comparison with small angle X-ray scattering (SAXS), for silver nanoparticles[47]. Here, direct evidence of the aggregation state of the particles in their native hydrated condition was given by bright-field TEM of cryo-prepared samples, again avoiding selection bias by imaging pre-determined areas.

The binding of poly(MPC) to the nanoparticles was visualized by positive staining using uranyl acetate, previously used to stain e.g. phosphorylcholine-containing surfactants[47,48]. Individual nanoparticles and their stained-polymer coronas were visualized by high-angular

aperture dark field scanning transmission electron microscopy (HAADF-STEM). To clearly distinguish iron from the uranium stain, energy-dispersive X-ray spectroscopy (EDX) linescans were taken across the particle and corona.

Dynamic Light scattering (DLS)

DLS measurements gave macroscale characterization of nanoparticle aggregation state, confirming the microscopic TEM results (see Supporting Information). Analysis was performed on samples of functionalized and non-functionalized nanoparticles prepared as for bright-field TEM.

Nanowires: poly(MPC) binding and stability analysis

Nanowires (2 mg) were collected by magnetic separation (as for nanoparticles above) and resuspended in water (200 μl), before addition to poly(MPC) solution (800 μl 6.25 mg/ml in water). The mixture was incubated overnight, with ultrasonication for the first 10 mins to destabilize pre-existing aggregates. Poly(MPC)-coated nanowires were collected by magnetic separation and rinsed 3 times in water to remove unbound polymer, with 10 mins ultrasonication at each stage. Control samples were prepared using water alone rather than poly(MPC) solution. Poly(MPC) binding to nanowires was evaluated using uranyl acetate staining and HAADF-STEM and STEM-EDX as for spherical nanoparticles. The aggregation state of nanowires was determined using a combination of scanning electron microscopy (SEM), performed on dried samples and *in situ* solution-phase bright-field reflectance mode optical microscopy (protocols in Supporting Information), as we have previously demonstrated for silver nanowires and multi-walled carbon nanotubes[49,50].

Nanowire cytotoxicity assays

The effect of poly(MPC) coating on cytotoxicity of nanowires was determined for the case of the core-shell iron/iron oxide nanowires. Cell viability studies were carried out on HCT 116 colon cancer cells incubated with poly(MPC)-coated and non-coated nanowires at concentrations of 250 and 500 nanowires per cell, broadly consistent with the concentration range in which cytotoxic effects have previously been observed for iron nanowires[46]. No cytotoxicity was observed for any sample up to 3 h, hence results presented are from overnight incubation. Cell survival was determined by an Alamar Blue assay (ThermoFisher), with each condition replicated in quadruplicate. (Further details in SI.)

Results and Discussion

Poly(MPC) binding to magnetite nanoparticle surfaces

The first requirement for poly(MPC) to effectively stabilize iron oxide nanostructures is that it must adsorb to the nanostructure surface, as is anticipated from the large number of phosphate groups along the polymer length. To test this, magnetite nanoparticles (Fe_3O_4, diameter 20 nm) were incubated with poly(MPC) (Mn = 8,500 Da) in aqueous solution. To visualize the polymer corona around the nanoparticles, we used analytical STEM, enhancing contrast via uranium-staining of the phosphorylcholine groups. A surface-adsorbed layer of poly(MPC) is clearly visible as a bright halo at the nanoparticle edge (HAADF-STEM, Fig. 2). This feature is lacking in non-functionalized poly(MPC) samples. The identity of the corona is confirmed by STEM-EDX linescans, which distinguish the iron-rich nanoparticle from the uranium-stained polymer corona (Fig. 2). It is important to note, that although such adsorption of poly(MPC) is in principle a logical consequence of the polymer structure, it has not been previously attempted.

Stabilization of individual magnetite nanoparticles by poly(MPC) adsorption

Surface-adsorbed poly(MPC) is clearly an excellent candidate to stabilize magnetite nanoparticles against aggregation and flocculation, in common with the long history of hydrophilic polymers as stabilizers for aqueous colloids and nanostructures, back to gum Arabic-stabilized black ink in ancient Egypt[51]. However, the generation of individual nanoparticles is not guaranteed, as other outcomes can include polymer-induced flocculation due to bridging between[52] and the stabilization of small multi-particle groups as for the carbohydrate-iron oxide MRI contrast agents discussed above[17].

The effect of poly(MPC) (M_n = 8,500 Da) functionalization on magnetite nanoparticle stability was determined by bright-field TEM (Fig. 3A top row). It can clearly be seen that the poly(MPC) coating greatly increases the likelihood of magnetite particles existing as individuals, whereas uncoated samples are dominated by aggregates. The high dominance of individual nanoparticles is confirmed by statistical measurements of aggregate size determined from images (N > 500 nanoparticles per condition across multiple fields of view) (Fig. 3B). The large majority of poly(MPC)-coated nanoparticles (>60%) exist as individuals, with very few (< 5%) in aggregates of >5 particles, whereas such aggregates are by far the dominant species (>60%) in the absence of poly(MPC).

The above measurements (Fig. 3) were determined using samples deposited on TEM grids and air-dried, with the simplicity of this protocol enabling high-quality statistics across a large number of particles. This methodology has been previously validated (for silver nanoparticles) by direct comparison with *in situ* small-angle X-ray scattering (SAXS)[47]; note also that any drying effects would be expected to increase rather than decrease aggregation. To further confirm the effect of poly(MPC) in stabilizing and individualizing nanoparticles, we directly characterized of nanoparticle-poly(MPC) solutions in the hydrated state, using both cryo-TEM

and dynamic light scattering (DLS). Cryo-TEM images (Fig 3A, bottom row) shows that individual nanoparticles are the dominant species for poly(MPC)-coated nanoparticles, whereas aggregates dominate for uncoated samples, reproducing the result from deposited samples. Finally, DLS was used as a technique that measures a far larger population of particles than TEM. Once again, the degree of aggregation was dramatically reduced upon coating with poly(MPC) (Fig. 3C).

Disaggregation of magnetic iron oxide nanowires via poly(MPC) adsorption

Here, we extend the poly(MPC) homopolymer adsorption approach demonstrated in the previous section to high-aspect ratio iron oxide nanowires, showing that it can disaggregate nanowires and enhance biocompatibility by reducing cytotoxicity. To determine the efficacy of poly(MPC) across iron oxide surfaces with potential differences in surface structure and chemistry, two nanowire systems were investigated.

To generate the ideal properties for biomedical application, we first developed a novel system of super-paramagnetic iron oxide nanowires, generated by templated electrodeposition from a mixed solution of ammonium iron(II) sulfate ($(NH_4)_2Fe(SO_4)_2$) and potassium acetate (CH_3COOK), with the temperature held at 90°C to favor magnetite formation. Successful release and removal of template residue was demonstrated by XPS (Fig S.5B). Following release, TEM revealed a population of polycrystalline nanowires (Fig S.4A) with length of 3.31 ± 0.12 μm, diameter of 199 ± 2 nm (Fig S.3E,F). The wires are super-paramagnetic, with a magnetic moment at saturation of 83 ± 5 emu/g (Fig S.6). This super-paramagnetism must arise from the polycrystalline structure, with each crystallite acting as an independent super-paramagnetic domain. Importantly, electrodeposited super-paramagnetic nanowires have not previously been

reported, with the only previous templated electrodeposition of magnetite delivering ferromagnetic properties with a different deposition chemistry and much thicker wires[53].

Structurally, while the protocol was designed to deposit magnetite (Fe_3O_4), the presence of maghemite (γ-Fe_2O_3) can also be seen from X-ray diffraction XRD (Fig S.4D), XPS (Fig S.5C) and the value of the saturation magnetic moment, which is intermediate between the two phases. In addition, comparison of the Fe 2*p* core level of a mixed iron oxide measured by Biesinger *et al*.[54], shows significant similarity to our measurement, with the exception of our system not displaying a metallic Fe peak.

As a contrast to the super-paramagnetic magnetite-maghemite system, poly(MPC) stabilization was also investigated using ferromagnetic nanowires of similar length. These are a core-shell iron-iron oxide system, generated by deposition of iron into porous templates (see Methods), as described previously.

The binding of poly(MPC) to the nanowire surfaces was visualized by STEM with uranyl acetate-staining of the phosphorycholine groups, as for the magnetite nanoparticles above (Fig. 4). Both nanowire systems show clear adsorption of poly(MPC). This is evidenced in HAADF-STEM by a bright halo at the nanowire edge (Fig 4A, lower panels). EDX linescans confirm that this is associated with a high uranium signal, indicating a layer of poly(MPC) at the nanowire surface (Fig 4B, lower panels).

The aggregation state of the nanowires was strongly modified by poly(MPC) (Fig. 5). In the absence of poly(MPC), both nanowire systems formed large aggregates, visible as disordered bunches of nanowires in scanning electron microscopy. This is consistent with expectation for these ferromagnetic nanowires, as both short-range surface forces and the permanent magnetic moment of the nanowires tend to favor aggregation[55]. The existence of such aggregates in the

solution state is also shown by reflectance mode optical microscopy, where they show up as large dark features[49]. Coating with poly(MPC) removes these aggregates, with no or very few such dark patches visible in the optical reflectance image. It should be emphasized that such disassembly of pre-existing aggregates is a strong indicator of a molecule's stabilizing power.

Higher resolution investigation by SEM confirmed the disappearance of the very large aggregates that dominate the non-functionalized samples (Fig. 5). The resulting disaggregated samples contain both individualized nanowires and also very small groups of nanowires. In the magnetite-maghemite case in particular, these small groups are predominantly end-to-end chains. Although these are reminiscent of magnetically-driven end-to-end assembly such as has been observed for nickel nanowires[56,57], this is unlikely due to the wires' paramagnetic nature; rather the end-to-end interactions are likely to be driven by other factors such as disruption of the stabilization layer by the less flat geometry at the nanowire end.

Poly(MPC) reduces nanowire cytotoxicity

Antifouling polymers suppress non-specific cell-nanostructure interactions, and should thus reduce cytotoxicity of nanostructures where that toxicity arises from direct uptake or adhesion of the nanostructures to the cell surface. To see whether poly(MPC) plays such a role in the present system, we investigated its effect on nanostructure cytotoxicity. Magnetite and maghemite are highly biocompatible, but there is evidence of low level cytotoxicity in nanowires (core-shell iron-iron oxide)[46], hence these were selected.

Cytotoxicity studies were carried out using HCT 116 colon cancer cells, with the AlamarBlue metabolic assay as a measure of % cell survival (Fig. 6). Visual observation in cell culture solutions again indicated a substantially reduced presence of nanowire aggregates for poly(MPC)-coated nanowires, as opposed to non-coated wires (Fig 6A). Non-coated wires

induced a significant decrease in cell survival at a concentration of 500 nanowires per cell after overnight incubation (< 80% of control value, $p < 0.001$, 4 repetitions), highly consistent with previous observations[46] (Fig 6B). This cytotoxicity substantially disappears ($p < 0.001$) for identical nanowires that are coated with poly(MPC). These experiments do not reveal the mechanism by which cytotoxicity is reduced. It should be noted however in this context, that the poly(MPC) layer could in principle inhibit uptake of nanoparticles by sterically screening interactions between cell surface lipids and the positively-charged surface of bare magnetite[58] that have been implicated in uptake of positively-charged nanoparticles. Alternatively, poly(MPC) could reduce cytotoxicity by influencing the speed of nanowire dissolution in the lysosome[59], or by reducing potential cytotoxic effects arising from aggregation. Regardless of mechanism, these results clearly establish poly(MPC) as a reagent to increase the already biocompatibility of iron oxide nanostructures.

*Click-functionalization via poly(MPC-*co*-PMA) random co-polymerization*

To enhance the applicability of poly(MPC)-stabilized nanostructures in applications such as cell-targeting, we now demonstrate the incorporation of an alkyne (C≡C) group that enables functionalization via the well known 'click' method, without compromising the simplicity of the synthesis. Specifically, we generate a random copolymer of poly(MPC-*co*-propagryl methacrylate), poly(MPC-*co*-PMA).

To synthesize poly(MPC-*co*-PMA), a first step was to perform the MPC polymerization in ethanol as a suitable co-solvent for the two monomers (as above). Alkyne groups have proved challenging to incorporate into (meth)acrylate ATRP, with the possibility that they may interfere with the ATRP control/catalysis process leading to attempts to polymerize them in silane-protected form, also without success due to deprotecting side-reactions[38]. Here, as an alternative,

we trial a simple ATRP co-polymerization of PMA with MPC, using the copper-bpy catalyst system as for the MPC co-monomer. Preliminary experiments indicated that PMA does not in fact prevent effective polymerization. Optimization of the process showed that a 1:2 ratio of PMA : MPC in the reaction mixture delivered a polymer with a significant number of functionalizable alkyne groups, while maintaining reasonable dispersity.

Synthesis of poly(MPC-*co*-PMA) is demonstrated by GPC, and functionalization with an azide-functionalized fluorescent dye (azide-Fluor 545, Sigma Aldrich). GPC shows that ATRP of MPC and PMA in ethanol under the same conditions as MPC alone (8.5 kDa, Mn/Mw = 1.18) generates a slightly increased molecular weight and dispersity (11.5 kDa, Mn/Mw = 1.26, Fig S.1). The resulting polymer successfully incorporates some alkyne functional groups, clearly shown by the copper-catalyzed addition of azide-Fluor545. This is demonstrated by GPC, comparing refractive index change (RI) associated primarily with the polymer with UV-adsorption that indicates the presence of the dye (Fig. 7A). For azide-Fluor545dye-reacted poly(MPC-*co*-PMA), these two signals rise and fall in consort with elution time, showing that the polymer has been successfully reacted with the dye. This stands in contrast to poly(MPC) incubated with azide-Fluor545 under the same conditions, which shows no UV-absorbance. Quantification shows that the number of PMA residues per polymer chain (~ 39 monomers) is ≥2, i.e. > 5% incorporation, and indeed a large ratio of pMPC to PMA is desired to retain the stabilization functionality.

The ability of this molecule to deliver simultaneous stabilization and functionalization of magnetic iron nanostructures was demonstrated using spherical magnetite nanoparticles (20 nm, as above). Clearly the strength of click-chemistry is the ability to attach a range of (bio)molecules; as a proof-of-principle, azide-Fluor545 dye was again used. Specifically,

magnetite nanoparticles (20 nm) were incubated with poly(MPC-*co*-PMA-azide-Fluor545). The polymer binds to the nanoparticles, with a bright halo at the particle surface in uranium-stained HAADF-STEM, exactly as for poly(MPC) above (Fig. 7C). Equally, polymer-coated magnetite nanoparticles are individualized and stabilized as for poly(MPC) (Fig. 7D, cryo-TEM, comparing images of polymer-coated and non-coated particles). Evidently, the incorporation of PMA at this level does not interfere with these properties. The incorporation of functionality is successful, as shown in this case by UV-vis spectroscopy of polymer-coated nanoparticles, confirming the presence of the Fluor545 dye (Fig. 7B, unbound polymer was removed using a magnetic separation). Quantification gave values of ~4 dye molecules per nanoparticle, corresponding to ~2 polymer chains per nanoparticle. Clearly this number would be greatly increased for larger nanostructures such as the nanowires studied, whose surface area is ~ 600 times greater.

Conclusions

We have demonstrated a novel approach to stabilizing biocompatible magnetic iron oxide nanostructures, using one-pot and one-step homopolymerization or simultaneous co-polymerization of poly(MPC). Nanostructures are thus polymer-coated via a strongly-binding phosphate moiety, with no need for end-functionalized polymers, complex architectures or multistep processes. This approach combines the ease-of-use of clinically-used long-chain carbohydrates with stronger anchoring and the improved definition and flexibility of a synthetic polymer. We have validated poly(MPC)-stabilization across spherical nanoparticles and high-aspect ratio nanowires, with clear evidence that poly(MPC) combines the required attributes of binding iron oxide surfaces, stabilizing against aggregation and enhancing biocompatibility. Functionality via a click moiety has been incorporated, without compromising stabilization, or

ease-of-use. In conclusion, we have demonstrated that poly(MPC) is a candidate stabilizer for a new generation of manufacturable high-precision biocompatible magnetic nanomaterials.

Supporting Information: Additional materials and methods; Characterization of electrodeposited magnetite-maghemite nanowires.

Acknowledgements We acknowledge funding from a KAUST Partnership grant (JK, MMS, IED, AEP, GL, PC, JEP).

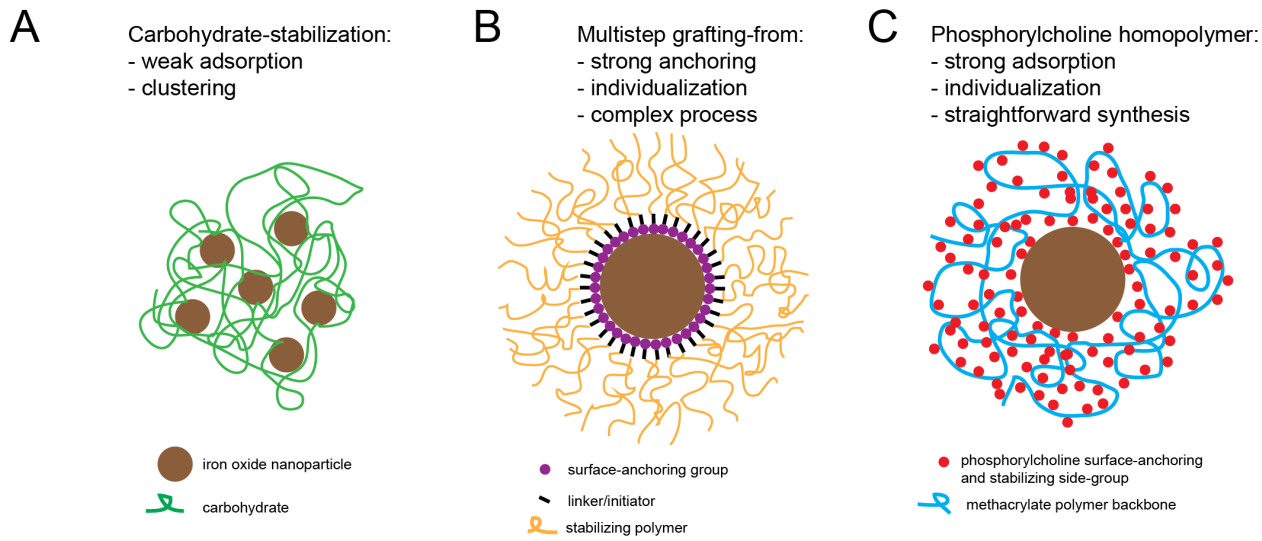


Figure 1. A) Schematic showing major approaches to iron oxide nanostructure stabilization with advantages and disadvantages. (A) Carbohydrate stabilization, e.g. commercial dextran reagents; (B) Multistep grafting-from; (C) Direct adsorption of phosphorylcholine homopolymer (MPC) that simultaneously binds surface and acts as stabilizing and antifouling layer. Acknowledgement: (A) Left and Center panels redrawn after Ref 17, copyright Royal Society of Chemistry 2011, used with permission.

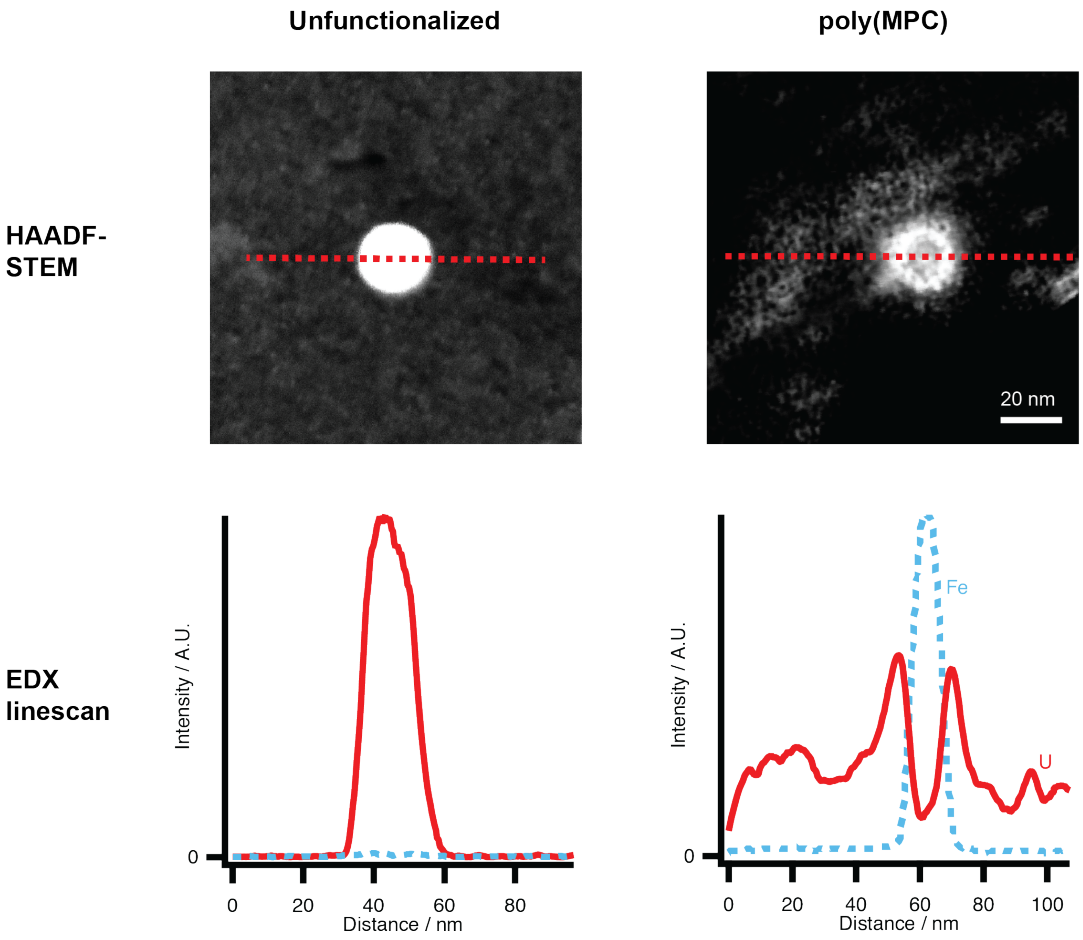


Figure 2. Poly(MPC) adsorption to magnetite nanoparticle surfaces. The adsorbed polymer corona is visualized by STEM in combination with uranium staining of the phosphorycholine groups. Poly(MPC)-functionalized and non-functionalized magnetite nanoparticles are visualized by HAADF-STEM (top row). The uranium-stained polymer corona is clearly distinguished from the iron-rich nanoparticle by an elemental microanalysis (STEM-EDX) linescan (bottom row, linescan region marked in HAADF-STEM image). Representative image from >5 particles for each condition.

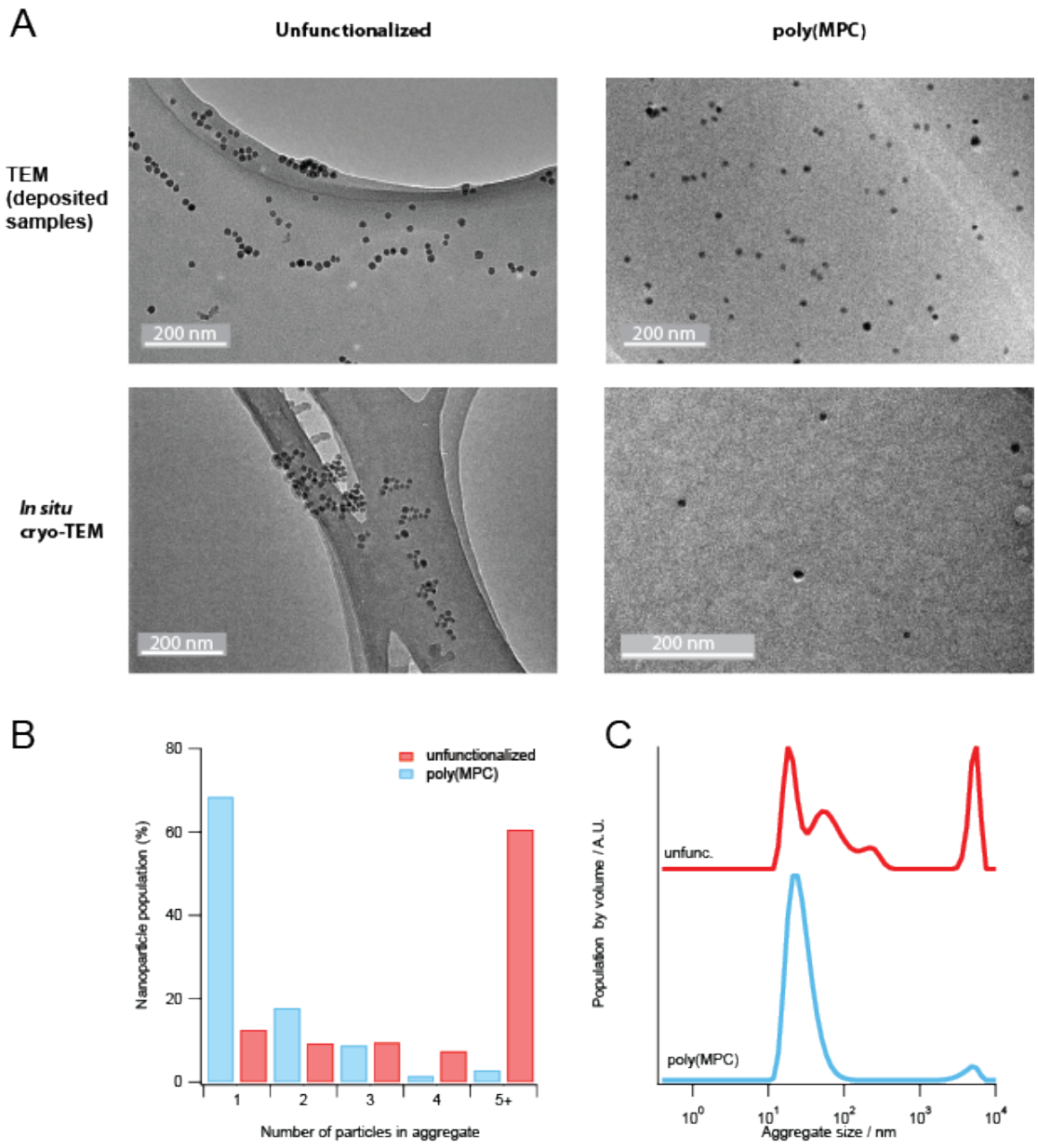


Figure 3. Stabilization of magnetite nanoparticles by surface-adsorbed poly(MPC). (A) Representative images with (right) and without (left) poly(MPC) coating of magnetite (bright-field TEM). Top row shows samples dry-deposited on TEM grid, second row shows confirmation by *in situ* cryo-TEM (see Methods). (B) Statistical distribution of aggregate size, measured over N > 500 nanoparticles per condition (dry-deposited sample). (C) Dynamic light scattering (DLS) of the same solutions at ambient temperature.

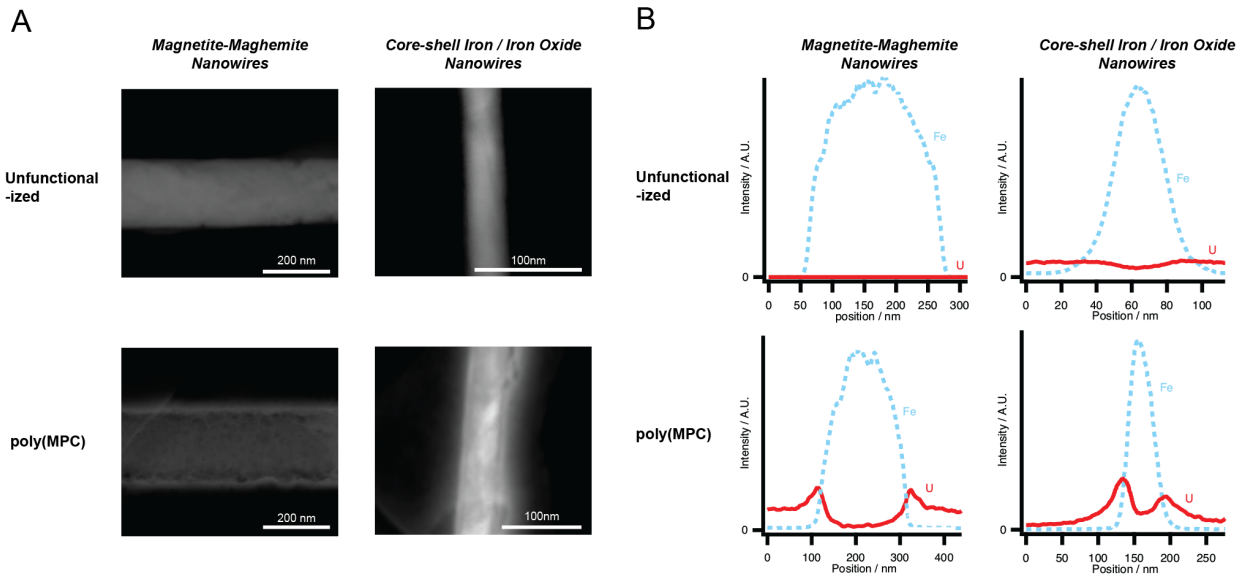


Figure 4. Poly(MPC) adsorption to iron oxide nanowires, visualized via uranium-staining of phosphorylcholine groups. (A) HAADF–STEM of poly(MPC)–functionalized and non-functionalized nanowires. (B) EDX-linescans across representative nanowire sections.

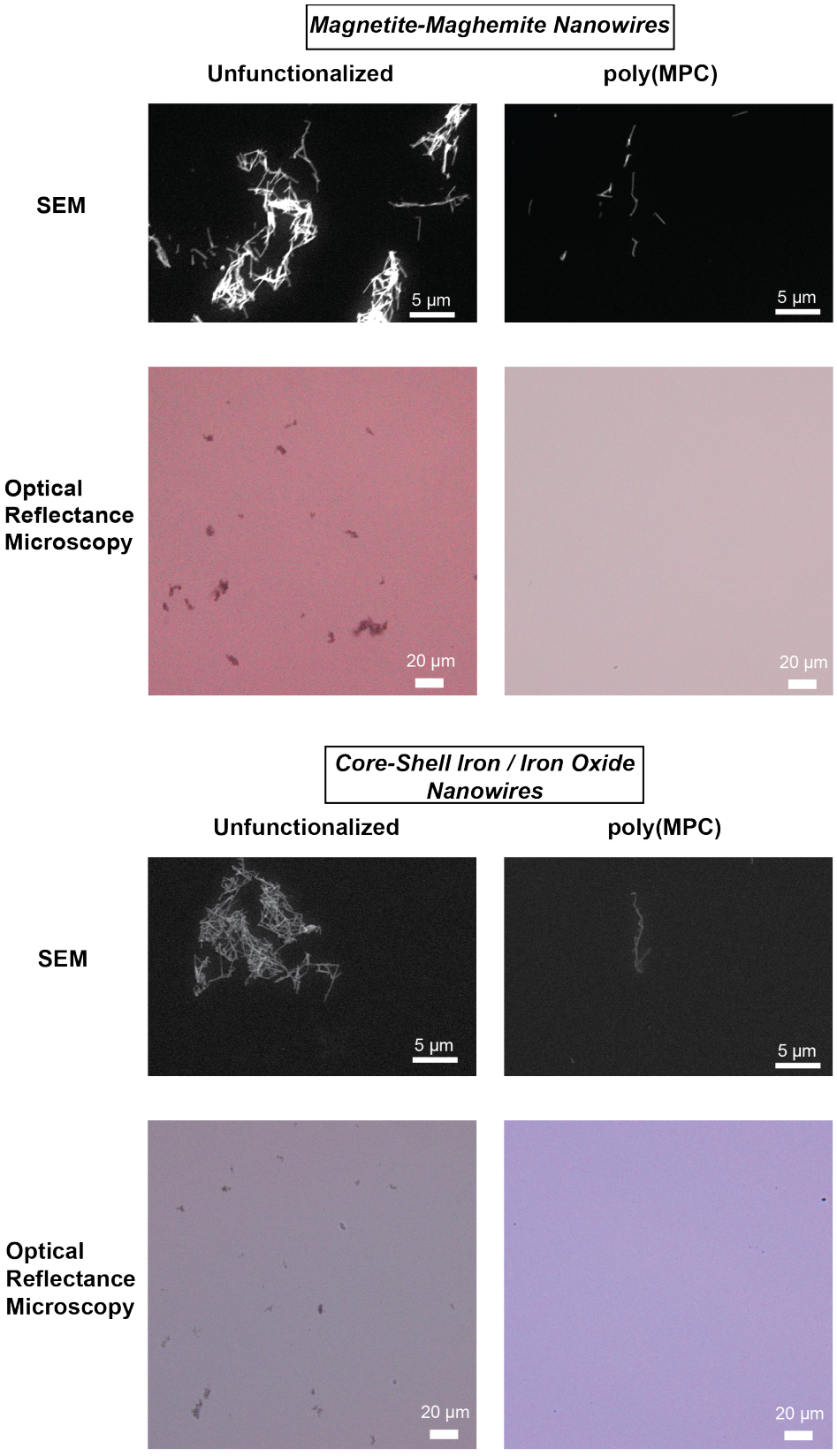

Magnetite-Maghemite Nanowires
Unfunctionalized
poly(MPC)
SEM
5 µm
5 µm
Optical Reflectance Microscopy
20 µm
20 µm
Core-Shell Iron / Iron Oxide Nanowires
Unfunctionalized
poly(MPC)
SEM
5 µm
5 µm
Optical Reflectance Microscopy
20 µm
20 µm

Figure 5. Disaggregation of magnetic nanowires with iron oxide surfaces by poly(MPC). Two different nanowire systems, magnetite-maghemite (left panel) and core shell iron/iron oxide (right panel) are imaged by SEM (top row) and solution-phase optical reflectance microscopy (bottom row). Non-functionalized nanowires (left column of each panel) are compared with poly(MPC)-functionalized nanowires (right column of each panel) in each case. Large aggregates formed by unfunctionalized nanowires, directly visible by SEM, manifest as dark patches in the optical reflectance micrographs.

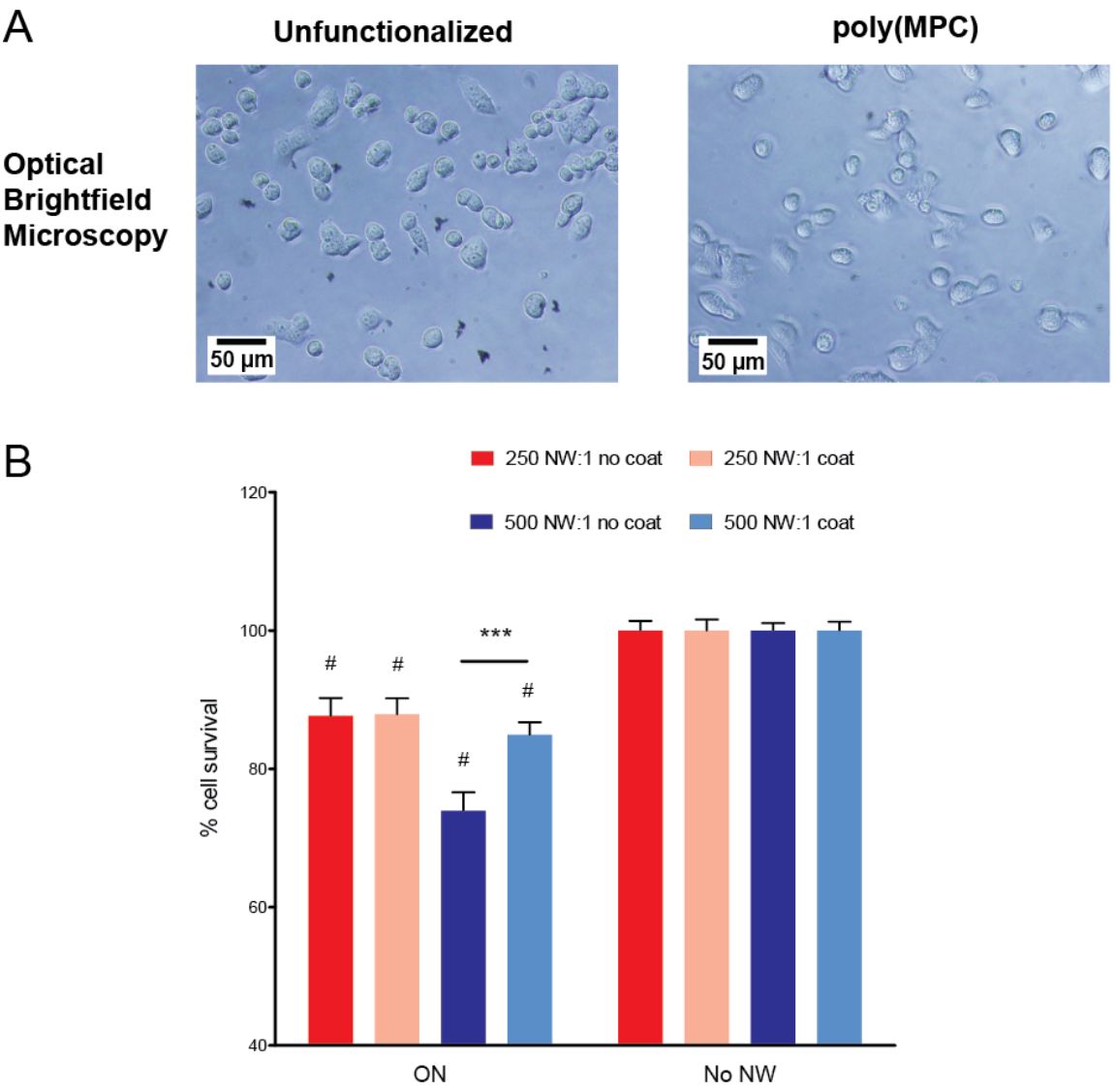


Figure 6. Cytocompatibility of poly(MPC)-coated and non-coated iron oxide nanowires. A) Brightfield optical micrographs of cells in contact with unfunctionalized and poly(MPC)-coated core-shell iron / iron oxide nanowires. B) Incubation of AlamarBlue viability assay on HCT 116 colon cancer cells incubated with either 250 or 500 nanowires/cell overnight (ON). The cell viability is reduced when cells are incubated with 500 non-coated nanowires per cell, but not when the nanowires are poly(MPC)-coated. #P<0.05 vs no-nanowire internal control; ***P<0.001 vs uncoated control.

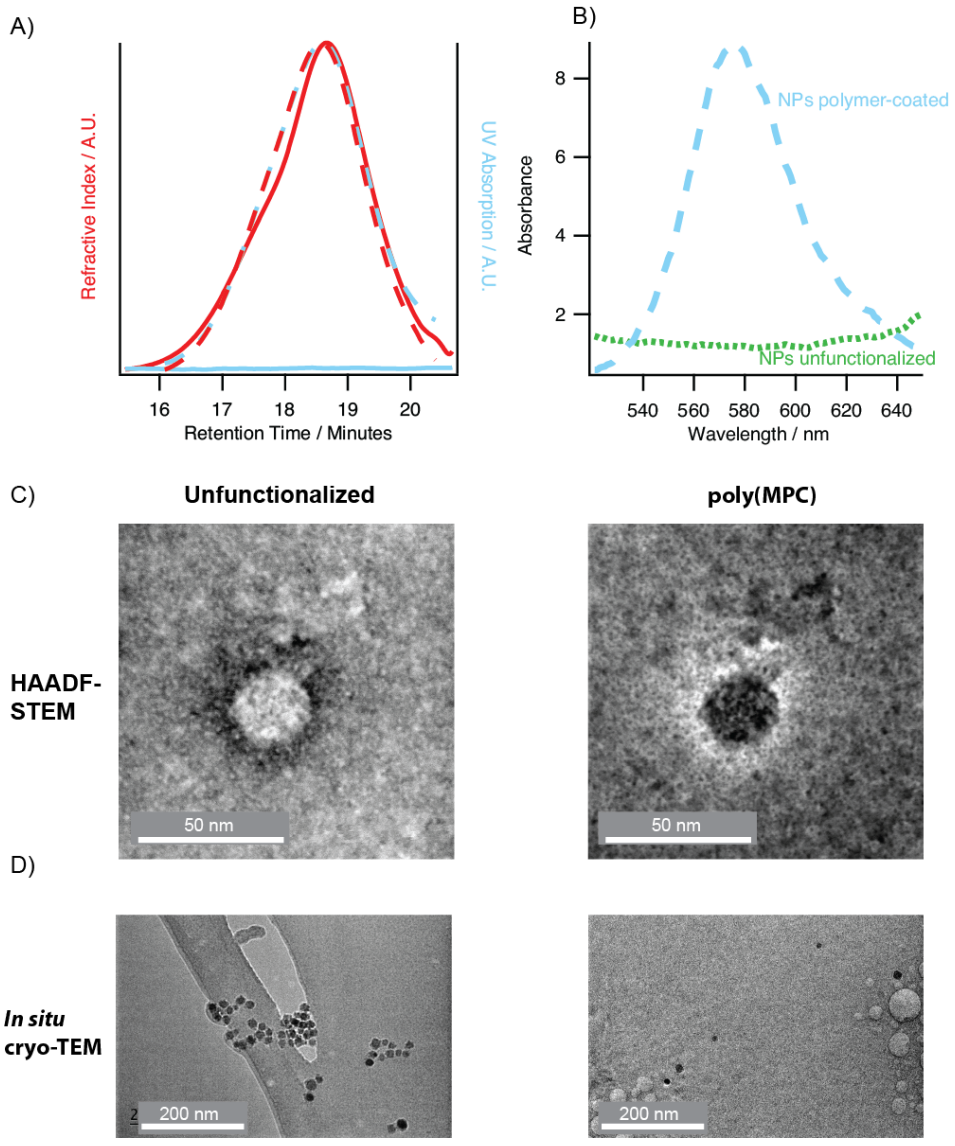


Figure 7. Functional nanoparticles via alkyne-azide click chemistry. A) Conjugation of azide-Fluor545 dye to poly(MPC-co-PMA) demonstrated by direct correlation between refractive index (RI, dashed red line) and UV absorption (dashed blue line) signals in GPC; solid lines show RI (red) and UV (blue) signal from unlabeled poly(MPC-co-PMA). (B) UV-vis spectroscopy of magnetically separated nanoparticles functionalized with poly(MPC-co-PMA) in comparison with unfunctionalized particles. (C) Poly(MPC-co-PMA) binding to magnetite

nanoparticle surface imaged by HAADF-STEM with uranium staining of phosphorylcholine groups, shown as white color; deposited samples of unfunctionalized and poly(MPC-co-MPA)-functioanlized nanoparticles. (D) *In situ* aqueous cryo-TEM of poly(MPC-co-PMA) coated versus uncoated nanoparticles, showing the change in aggregation state.

References

(1) Ling, D.; Lee, N.; Hyeon, T. Chemical Synthesis and Assembly of Uniformly Sized Iron Oxide Nanoparticles for Medical Applications. *Acc. Chem. Res.* **2015**, *48* (5), 1276–1285.

(2) Wu, J.; Wei, X.; Gan, J.; Huang, L.; Shen, T.; Lou, J.; Liu, B.; Zhang, J. X. J.; Qian, K. Multifunctional Magnetic Particles for Combined Circulating Tumor Cells Isolation and Cellular Metabolism Detection. *Adv. Funct. Mater.* **2016**, *26* (22), 4016–4025.

(3) Liu, W.; Nie, L.; Li, F.; Aguilar, Z. P.; Xu, H.; Xiong, Y.; Fu, F.; Xu, H. Folic Acid Conjugated Magnetic Iron Oxide Nanoparticles for Nondestructive Separation and Detection of Ovarian Cancer Cells From Whole Blood. *Biomater. Sci.* **2016**, *4* (1), 159–166.

(4) Bhana, S.; Lin, G.; Wang, L.; Starring, H.; Mishra, S. R.; Liu, G.; Huang, X. Near-Infrared-Absorbing Gold Nanopopcorns with Iron Oxide Cluster Core for Magnetically Amplified Photothermal and Photodynamic Cancer Therapy. *ACS Appl. Mater. Interfaces* **2015**, *7* (21), 11637–11647.

(5) Wang, C.; Xu, H.; Liang, C.; Liu, Y.; Li, Z.; Yang, G.; Cheng, L.; Li, Y.; Liu, Z. Iron Oxide @ Polypyrrole Nanoparticles as a Multifunctional Drug Carrier for Remotely Controlled Cancer Therapy with Synergistic Antitumor Effect. *ACS Nano* **2013**, *7* (8), 6782–6795.

(6) Guardia, P.; Di Corato, R.; Lartigue, L.; Wilhelm, C.; Espinosa, A.; Garcia-Hernandez, M.; Gazeau, F.; Manna, L.; Pellegrino, T. Water-Soluble Iron Oxide Nanocubes with High Values of Specific Absorption Rate for Cancer Cell Hyperthermia Treatment. *ACS Nano* **2012**, *6* (4), 3080–3091.

(7) Zhao, Q.; Wang, L.; Cheng, R.; Mao, L.; Arnold, R. D.; Howerth, E. W.; Chen, Z. G.; Platt, S. Magnetic Nanoparticle-Based Hyperthermia for Head & Neck Cancer in Mouse Models. *Theranostics* **2012**, *2* (1), 113–121.

(8) Ai, H.; Flask, C.; Weinberg, B.; Shuai, X. T.; Pagel, M. D.; Farrell, D.; Duerk, J.; Gao, J. Magnetite-Loaded Polymeric Micelles as Ultrasensitive Magnetic-Resonance Probes. *Adv. Mater.* **2005**, *17* (16), 1949–1952.

(9) Reddy, L. H.; Arias, J. L.; Nicolas, J.; Couvreur, P. Magnetic Nanoparticles: Design and Characterization, Toxicity and Biocompatibility, Pharmaceutical and Biomedical Applications. *Chem. Rev.* **2012**, *112* (11), 5818–5878.

(10) Lee, N.; Yoo, D.; Ling, D.; Cho, M. H.; Hyeon, T.; Cheon, J. Iron Oxide Based Nanoparticles for Multimodal Imaging and Magnetoresponsive Therapy. *Chem. Rev.* **2015**, *115* (19), 10637–10689.

(11) Johansson, F.; Jonsson, M.; Alm, K.; Kanje, M. Cell Guidance by Magnetic Nanowires. *Experimental Cell Res.* **2010**, *316* (5), 688–694.

(12) Cappallo, N.; Lapointe, C.; Reich, D. H.; Leheny, R. L. Nonlinear Microrheology of Wormlike Micelle Solutions Using Ferromagnetic Nanowire Probes. *Phys. Rev. E* **2007**, *76* (3), 031505.

(13) Hultgren, A.; Tanase, M.; Chen, C. S.; Meyer, G. J.; Reich, D. H. Cell Manipulation Using Magnetic Nanowires. *J. Appl. Phys.* **2003**, *93* (10), 7554–7556.

(14) Fratila, R. M.; Rivera-Fernández, S.; la Fuente, de, J. M. Shape Matters: Synthesis and Biomedical Applications of High Aspect Ratio Magnetic Nanomaterials. *Nanoscale* **2015**, *7* (18), 8233–8260.

(15) Kim, D.-H.; Rozhkova, E. A.; Ulasov, I. V.; Bader, S. D.; Rajh, T.; Lesniak, M. S.; Novosad, V. Biofunctionalized Magnetic-Vortex Microdiscs for Targeted Cancer-Cell Destruction. *Nature Mater.* **2010**, *9* (2), 165–171.
(16) Contreras, M.; Sougrat, R.; Zaher, A.; Ravasi, T.; Kosel, J. Non-Chemotoxic Induction of Cancer Cell Death Using Magnetic Nanowires. *Int. J. Nanomedicine* **2015**, *10* (1), 2141–2153.
(17) Amstad, E.; Textor, M.; Reimhult, E. Stabilization and Functionalization of Iron Oxide Nanoparticles for Biomedical Applications. *Nanoscale* **2011**, *3* (7), 2819.
(18) Fütterer, S.; Andrusenko, I.; Kolb, U.; Hofmeister, W.; Langguth, P. Structural Characterization of Iron Oxide/Hydroxide Nanoparticles in Nine Different Parenteral Drugs for the Treatment of Iron Deficiency Anaemia by Electron Diffraction (ED) and X-Ray Powder Diffraction (XRPD). *J. Pharmaceutical Biomed. Anal.* **2013**, *86*, 151–160.
(19) Wei, H.; Insin, N.; Lee, J.; Han, H.-S.; Cordero, J. M.; Liu, W.; Bawendi, M. G. Compact Zwitterion-Coated Iron Oxide Nanoparticles for Biological Applications. *Nano Lett.* **2012**, *12* (1), 22–25.
(20) Xie, J.; Xu, C.; Kohler, N.; Hou, Y.; Sun, S. Controlled PEGylation of Monodisperse Fe_3O_4 Nanoparticles for Reduced Non-Specific Uptake by Macrophage Cells. *Adv. Mater.* **2007**, *19* (20), 3163–3166.
(21) Sun, X.-Y.; Yu, S.-S.; Wan, J.-Q.; Chen, K.-Z. Facile Graft of Poly(2-Methacryloyloxyethyl Phosphorylcholine) Onto Fe_3O_4 Nanoparticles by ATRP: Synthesis, Properties, and Biocompatibility. *J. Biomed. Mater. Res., Part A* **2012**, *101A* (2), 607–612.
(22) Nguyen, T.-K.; Duong, H. T. T.; Selvanayagam, R.; Boyer, C.; Barraud, N. Iron Oxide Nanoparticle-Mediated Hyperthermia Stimulates Dispersal in Bacterial Biofilms and Enhances Antibiotic Efficacy. *Sci. Rep.* **2015**, *5*, 18385.
(23) Ishihara, K.; Aragaki, R.; Ueda, T.; Watenabe, A.; Nakabayashi, N. Reduced Thrombogenicity of Polymers Having Phospholipid Polar Groups. *J. Biomed. Mater. Res.* **1990**, *24* (8), 1069–1077.
(24) Ishihara, K.; Nomura, H.; Mihara, T.; Kurita, K.; Iwasaki, Y. Why Do Phospholipid Polymers Reduce Protein Adsorption? **1998**, *39* (2), 323–330.
(25) Jawanda, M.; Lai, B. F. L.; Kizhakkedathu, J. N.; Ishihara, K.; Narain, R. Linear and Hyperbranched Phosphorylcholine Based Homopolymers for Blood Biocompatibility. *Polym. Chem.* **2013**, *4* (10), 3140–3146.
(26) Ishihara, K.; Oshida, H.; Endo, Y.; Ueda, T.; Watanabe, A.; Nakabayashi, N. Hemocompatibility of Human Whole-Blood on Polymers with a Phospholipid Polar Group and Its Mechanism. *J. Biomed. Mater. Res.* **1992**, *26* (12), 1543–1552.
(27) Tateishi, T.; Kyomoto, M.; Kakinoki, S.; Yamaoka, T.; Ishihara, K. Reduced Platelets and Bacteria Adhesion on Poly(Ether Ether Ketone) by Photoinduced and Self-Initiated Graft Polymerization of 2-Methacryloyloxyethyl Phosphorylcholine. *J. Biomed. Mater. Res., Part A* **2014**, *102* (5), 1342–1349.
(28) Kim, Il, H.; Ishihara, K.; Lee, S.; Seo, J.-H.; Kim, H. Y.; Suh, D.; Kim, M. U.; Konno, T.; Takai, M.; Seo, J.-S. Tissue Response to Poly(L-Lactic Acid)-Based Blend with Phospholipid Polymer for Biodegradable Cardiovascular Stents. *Biomaterials* **2011**, *32* (9), 2241–2247.
(29) Takatori, Y.; Moro, T.; Kamogawa, M.; Oda, H.; Morimoto, S.; Umeyama, T.; Minami,

M.; Sugimoto, H.; Nakamura, S.; Karita, T.; Kim, J.; Koyama, Y.; Ito, H.; Kawaguchi, H.; Nakamura, K. Poly(2-Methacryloyloxyethyl Phosphorylcholine)-Grafted Highly Cross-Linked Polyethylene Liner in Primary Total Hip Replacement: One-Year Results of a Prospective Cohort Study. *J. Artific. Organs* **2013**, *16* (2), 170–175.

(30) Takatori, Y.; Moro, T.; Ishihara, K.; Kamogawa, M.; Oda, H.; Umeyama, T.; Kim, Y. T.; Ito, H.; Kyomoto, M.; Tanaka, T.; Kawaguchi, H.; Tanaka, S. Clinical and Radiographic Outcomes of Total Hip Replacement with Poly(2-Methacryloyloxyethyl Phosphorylcholine)-Grafted Highly Cross-Linked Polyethylene Liners: Three-Year Results of a Prospective Consecutive Series. *Mod. Rheumatol.* **2015**, *25* (2), 286–291.

(31) Yuan, J. J.; Armes, S. P.; Takabayashi, Y.; Prassides, K.; Leite, C. A. P.; Galembeck, F.; Lewis, A. L. Synthesis of Biocompatible Poly[2-(Methacryloyloxy)Ethyl Phosphorylcholine]-Coated Magnetite Nanoparticles. *Langmuir* **2006**, *22* (26), 10989–10993.

(32) Ivanov, Y. P.; Alfadhel, A.; Alnassar, M.; Perez, J. E.; Vazquez, M.; Chuvilin, A.; Kosel, J. Tunable Magnetic Nanowires for Biomedical and Harsh Environment Applications. *Sci. Rep.* **2016**, *6*, 24189.

(33) Rostovtsev, V. V.; Green, L. G.; Fokin, V. V.; Sharpless, K. B. A Stepwise Huisgen Cycloaddition Process: Copper(I)-Catalyzed Regioselective "Ligation" of Azides and Terminal Alkynes. *Angew. Chem.* **2002**, *41* (14), 2596–2599.

(34) Malkoch, M.; Vestberg, R.; Gupta, N.; Mespouille, L.; Dubois, P.; Mason, A. F.; Hedrick, J. L.; Liao, Q.; Frank, C. W.; Kingsbury, K.; Hawker, C. J. Synthesis of Well-Defined Hydrogel Networks Using Click Chemistry. *Chem. Commun.* **2006**, 2774–2776.

(35) Jiang, Y.; Chen, J.; Deng, C.; Suuronen, E. J.; Zhong, Z. Click Hydrogels, Microgels and Nanogels: Emerging Platforms for Drug Delivery and Tissue Engineering. *Biomaterials* **2014**, *35* (18), 4969–4985.

(36) Boeggeman, E.; Ramakrishnan, B.; Pasek, M.; Manzoni, M.; Puri, A.; Loomis, K. H.; Waybright, T. J.; Qasba, P. K. Site Specific Conjugation of Fluoroprobes to the Remodeled Fc N-Glycans of Monoclonal Antibodies Using Mutant Glycosyltransferases: Application for Cell Surface Antigen Detection. *Bioconjugate Chem.* **2009**, *20* (6), 1228–1236.

(37) Sumerlin, B. S.; Tsarevsky, N. V.; Louche, G.; Lee, R. Y.; Matyjaszewski, K. Highly Efficient "Click" Functionalization of Poly(3-Azidopropyl Methacrylate) Prepared by ATRP. *Macromolecules* **2005**, *38* (18), 7540–7545.

(38) Chen, X.; McRae, S.; Parelkar, S.; Emrick, T. Polymeric Phosphorylcholine–Camptothecin Conjugates Prepared by Controlled Free Radical Polymerization and Click Chemistry. *Bioconjugate Chem.* **2009**, *20* (12), 2331–2341.

(39) Lobb, E. J.; Ma, I.; Billingham, N. C.; Armes, S. P.; Lewis, A. L. Facile Synthesis of Well-Defined, Biocompatible Phosphorylcholine-Based Methacrylate Copolymers via Atom Transfer Radical Polymerization at 20 °C. *J. Am. Chem. Soc.* **2001**, *123* (32), 7913–7914.

(40) Ma, I. Y.; Lobb, E. J.; Billingham, N. C.; Armes, S. P.; Lewis, A. L.; Lloyd, A. W.; Salvage, J. Synthesis of Biocompatible Polymers. 1. Homopolymerization of 2-Methacryloyloxyethyl Phosphorylcholine via ATRP in Protic Solvents: an Optimization Study. *Macromolecules* **2002**, *35* (25), 9306–9314.

(41) Yuan, B.; Chen, Q.; Ding, W.-Q.; Liu, P.-S.; Wu, S.-S.; Lin, S.-C.; Shen, J.; Gai, Y. Copolymer Coatings Consisting of 2-Methacryloyloxyethyl Phosphorylcholine and 3-

Methacryloxypropyl Trimethoxysilane via ATRP to Improve Cellulose Biocompatibility. *ACS Appl. Mater. Interfaces* **2012**, *4* (8), 4031–4039.
(42) Masuda, H.; Fukuda, K. Ordered Metal Nanohole Arrays Made by a 2-Step Replication of Honeycomb Structures of Anodic Alumina. *Science* **1995**, *268* (5216), 1466–1468.
(43) Nielsch, K.; Muller, F.; Li, A. P.; Gosele, U. Uniform Nickel Deposition Into Ordered Alumina Pores by Pulsed Electrodeposition. *Adv. Mater.* **2000**, *12* (8), 582–586.
(44) Pirota, K.; Navas, D.; Hernandez-Velez, M.; Nielsch, K.; Vazquez, M. Novel Magnetic Materials Prepared by Electrodeposition Techniques: Arrays of Nanowires and Multi-Layered Microwires. *J. Alloys Compd.* **2004**, *369* (1-2), 18–26.
(45) Perez, J. E.; Contreras, M. F.; Vilanova, E.; Felix, L. P.; Margineanu, M. B.; Luongo, G.; Porter, A. E.; Dunlop, I. E.; Ravasi, T.; Kosel, J. Cytotoxicity and Intracellular Dissolution of Nickel Nanowires. *Nanotoxicology* **2016**, *10* (7), 871–880.
(46) Song, M.-M.; Song, W.-J.; Bi, H.; Wang, J.; Wu, W.-L.; Sun, J.; Yu, M. Cytotoxicity and Cellular Uptake of Iron Nanowires. *Biomaterials* **2010**, *31* (7), 1509–1517.
(47) Leo, B. F.; Chen, S.; Kyo, Y.; Herpoldt, K.-L.; Terrill, N. J.; Dunlop, I. E.; McPhail, D. S.; Shaffer, M. S.; Schwander, S.; Gow, A.; Zhang, J.; Chung, K. F.; Tetley, T. D.; Porter, A. E.; Ryan, M. P. The Stability of Silver Nanoparticles in a Model of Pulmonary Surfactant. *Environ. Sci. Technol.* **2013**, *47* (19), 11232–11240.
(48) Hajibagheri, M. Electron Microscopy: Methods and Protocols. *Methods Mol. Biol. N. Y., N.Y., U. S.* **1999**, *117*.
(49) Theodorou, I. G.; Botelho, D.; Schwander, S.; Zhang, J.; Chung, K. F.; Tetley, T. D.; Shaffer, M. S. P.; Gow, A.; Ryan, M. P.; Porter, A. E. Static and Dynamic Microscopy of the Chemical Stability and Aggregation State of Silver Nanowires in Components of Murine Pulmonary Surfactant. *Environ. Sci. Technol.* **2015**, *49* (13), 8048–8056.
(50) Goode, A. E.; Gonzalez Carter, D. A.; Motskin, M.; Pienaar, I. S.; Chen, S.; Hu, S.; Ruenraroengsak, P.; Ryan, M. P.; Shaffer, M. S. P.; Dexter, D. T.; Porter, A. E. High Resolution and Dynamic Imaging of Biopersistence and Bioreactivity of Extra and Intracellular MWNTs Exposed to Microglial Cells. *Biomaterials* **2015**, *70*, 57–70.
(51) Lucas, A. The Inks of Ancient and Modern Egypt. *Analyst* **1922**, *47* (550), 9–15.
(52) Cohen-Tannoudji, L.; Bertrand, E.; Bressy, L.; Goubault, C.; Baudry, J.; Klein, J.; Joanny, J.-F.; Bibette, J. Polymer Bridging Probed by Magnetic Colloids. *Phys. Rev. Lett.* **2005**, *94* (3), 038301.
(53) Terrier, C.; Abid, M.; Arm, C.; Serrano-Guisan, S.; Gravier, L.; Ansermet, J. P. Fe_3O_4 Nanowires Synthesized by Electroprecipitation in Templates. *J. Appl. Phys.* **2005**, *98* (8), 086102.
(54) Biesinger, M. C.; Payne, B. P.; Grosvenor, A. P.; Lau, L.; Gerson, A. R.; Smart, R. S. C. Resolving Surface Chemical States in XPS Analysis of First Row Transition Metals, Oxides and Hydroxides: Cr, Mn, Fe, Co and Ni. *Appl. Surf. Sci.* **2011**, *257* (7), 2717–2730.
(55) Safi, M.; Yan, M.; Guedeau-Boudeville, M.-A.; Conjeaud, H.; Garnier-Thibaud, V.; Boggetto, N.; Baeza-Squiban, A.; Niedergang, F.; Averbeck, D.; Berret, J.-F. Interactions Between Magnetic Nanowires and Living Cells: Uptake, Toxicity, and Degradation. *ACS Nano* **2011**, *5* (7), 5354–5364.
(56) Tanase, M.; Bauer, L. A.; Hultgren, A.; Silevitch, D. M.; Sun, L.; Reich, D. H.; Searson, P. C.; Meyer, G. J. Magnetic Alignment of Fluorescent Nanowires. *Nano Lett.* **2001**, *1* (3), 155–158.

(57) Tanase, M.; Felton, E. J.; Gray, D. S.; Hultgren, A.; Chen, C. S.; Reich, D. H. Assembly of Multicellular Constructs and Microarrays of Cells Using Magnetic Nanowires. *Lab Chip* **2005**, *5* (6), 598–605.
(58) Illés, E.; Tombácz, E. The Role of Variable Surface Charge and Surface Complexation in the Adsorption of Humic Acid on Magnetite. *Colloids Surf., A* **2003**, *230* (1-3), 99–109.
(59) Lartigue, L.; Alloyeau, D.; Kolosnjaj-Tabi, J.; Javed, Y.; Guardia, P.; Riedinger, A.; Péchoux, C.; Pellegrino, T.; Wilhelm, C.; Gazeau, F. Biodegradation of Iron Oxide Nanocubes: High-Resolution In Situ Monitoring. *ACS Nano* **2013**, *7* (5), 3939–3952.